Prediction of a strong polarizing field in thin film paraelectrics

Chiara Gattinoni ●[*]
Department of Chemical and Energy Engineering, London South Bank University,
London SE1 0AA, United Kingdom

Nicola A. Spaldin ●[†]
Department of Materials, ETH Zurich, CH-8093 Zürich, Switzerland

We demonstrate the existence of a polarizing field in thin films of insulators with charged ionic layers. The polarizing field derives from the same physics as the well-known depolarizing field that suppresses ferroelectric polarization in thin-film ferroelectrics, but instead drives thin films of materials that are centrosymmetric and paraelectric in their bulk form into a noncentrosymmetric, polar state. We illustrate the behavior using density-functional computations for perovskite-structure potassium tantalate, $KTaO_3$, which is of considerable interest for its high dielectric constant, proximity to a quantum critical point, and superconductivity. We then provide a simple recipe to identify whether a particular material and film orientation will exhibit the effect and develop an electrostatic model to estimate the critical thickness of the induced polarization in terms of basic material parameters. Our results provide practical guidelines for exploiting the electrostatic properties of thin-film ionic insulators to engineer novel functionalities for nanoscale devices.

I. INTRODUCTION

The surface charge associated with the spontaneous polarization in ferroelectrics is well known to cause a depolarizing field that can be particularly detrimental in the thin-film geometry desirable for microelectronic devices [1,2]. Incomplete screening of the surface charge, for example by metallic electrodes or surface adsorbates, can lead to the formation of domains [3], suppression or reorientation of the polarization [4], or even stabilization of a higher-energy nonpolar phase [5]. A huge amount of research and development effort has been invested in understanding the depolarizing behavior and minimizing its unfavorable effects.

In addition to the surface charge associated with bulk ferroelectric polarization, surface charge can occur in *centrosymmetric* insulators that contain charged ionic layers perpendicular to the surface plane. This layer surface charge $\sigma_{\text{layer}}^{\text{surf}}$ can be formalized in terms of a bulk layer polarization, as

$$\sigma_{\text{layer}}^{\text{surf}} = \vec{P}_{\text{layer}} \cdot \vec{n}, \tag{1}$$

where $\vec{P}_{\text{layer}}$ is the dipole moment per unit volume of the unit cell that tiles the semi-infinite plane containing the sur-

face in the centrosymmetric structure [6]. In centrosymmetric materials with a nonzero bulk layer polarization, the surface polar discontinuity arising from the layer charges needs to be compensated; the prototypical example is $LaAlO_3$, for which interfacial two-dimensional electron gases [7,8] and ionic reconstructions [9] have been experimentally observed.

In ferroelectric materials with charged ionic layers, these two components of the polarization interact, and the layer surface charge can add to or subtract from that from the spontaneous polarization, causing an interplay between polarization orientation and surface chemistry [10]. It was even demonstrated that, for the case of multiferroic bismuth ferrite, $BiFeO_3$, the surface charges from the layer and spontaneous polarizations almost exactly compensate (for appropriate choices of surface termination and spontaneous polarization orientation), leading to electrostatically stable ferroelectric thin films with zero depolarizing field even without metallic electrodes [11,12].

In this work we reveal an even more dramatic consequence of this interplay between layer and spontaneous polarization, showing computationally that the surface charge arising from the layer polarization causes a *polarizing field* that can *induce* ferroelectriclike polarization in a thin film of a material that is paraelectric in its bulk ground state.

Our model system is [001]-oriented perovskite-structure potassium tantalate, $KTaO_3$ [Fig. 1(a)]. Its formal ionic charges, K^{1+}, Ta^{5+}, and O^{2-}, lead to charged (001) layers and, correspondingly, to a nonzero bulk layer polarization, with positive and negative charges for (001) TaO_2 and KO surfaces [Figs. 1(b) and 1(c), respectively]. There has been considerable interest in its surface properties, with the layer surface charge shown to cause complex surface reconstructions
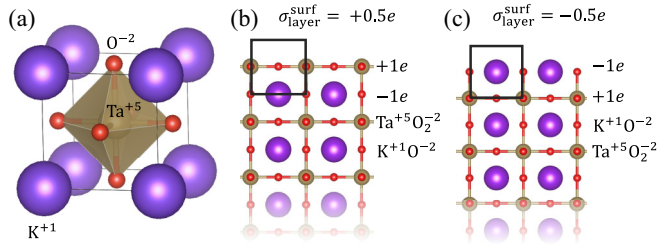
*gattinoc@lsbu.ac.uk
†nicola.spaldin@mat.ethz.ch

FIG. 1. Structure of bulk and thin-film KTaO$_3$. (a) Cubic perovskite unit cell. K, Ta, and O, with $+1$, $+5$, and -2 electronic charges e, are shown in purple, gold, and red, respectively. (b, c) Structures of the upper portions of [001]-oriented KTaO$_3$ slabs with flat TaO$_2$ (b) and KO (c) surfaces. The formal charges of the TaO$_2$ ($+1e$) and KO ($-1e$) layers are shown next to the layers. The black rectangles indicate the unit cells that tile the semi-infinite plane, used to calculate the surface charge $\sigma_{\text{layer}}^{\text{surf}}$ using Eq. (1) [see Supplemental Material (SM) [29]].

[13–16], including reports of a surface two-dimensional electron gas [17,18] and superconductivity with critical temperature depending on the choice of surface plane [19–21]. Finally, while it exhibits the centrosymmetric ideal cubic perovskite structure at all temperatures, its dielectric constant increases strongly as temperature is reduced, suggestive of quantum paraelectric behavior [22–24]. As a result, the internal energy difference between paraelectric and ferroelectric states is small, making it particularly suitable for demonstrating the effect that we describe.

II. METHODS

We performed density functional theory (DFT) calculations using the code Quantum Espresso [25] with the Perdew-Burke-Ernzerhof [26] exchange-correlation functional and Garrity-Bennet-Rabe-Vanderbilt (GBRV) pseudopotentials [27].

In order to accurately model the small energy and structural differences between paraelectric and ferroelectric KTaO$_3$, we sampled the five-atom unit cell using a $24 \times 24 \times 24$ Monkhorst-Pack k-point grid, and an energy cutoff of 75 Ry for the wave-function and 750 Ry for the charge density. For the slab calculations, we used a kinetic energy cutoff of 60 Ry for the wave function and 600 Ry for the charge density, an $8 \times 8 \times 1$ Monkhorst-Pack grid of k-points. The force convergence threshold for structural optimization was 10^{-4} eV/Å. Spin-orbit coupling was not included explicitly.

The optimized lattice constant for the metastable paraelectric unit cell was obtained by fixing the ions at their high-symmetry positions and fitting the Birch-Murnaghan equation to the energy calculated over a range of lattice parameters. To obtain the lowest-energy ferroelectric unit cell we minimized the Hellmann-Feynman stresses and forces.

We simulated slabs with a (1×1) area and with thicknesses between four and 15 unit cells. A 15-Å-thick vacuum separated periodic images along the [001] direction. A dipole correction was added in the vacuum. All slabs had KTaO$_3$ stoichiometry with one flat KO and one flat TaO$_2$ surface. We calculated the spontaneous polarization of the bulk and the layer-by-layer induced polarizations in the slabs by

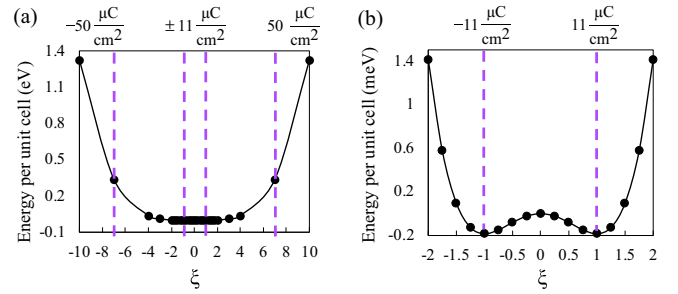FIG. 2. Calculated energy per unit cell as a function of polar distortion amplitude ξ for bulk KTaO$_3$. The lattice constants are fixed to those of the minimum energy structure, and the zero of energy is set to that of the centrosymmetric structure. (a) Over the range $-10 < \xi < 10$. (b) Close-up of the range $-2 < \xi < 2$. Note the different scales on the energy axes in the two cases. Vertical dashed purple lines indicate the ξ values corresponding to polarizations of 11 μC/cm^2 (at the bottom of the double well) and 50 μC/cm^2 (discussed later).

multiplying the displacement of each ion from its high-symmetry position by its Born effective charge value taken from Ref. [28] and normalizing to our calculated volume.

III. RESULTS

A. Bulk KTaO$_3$

Figure 2 shows the calculated energy per formula unit as a function of the amplitude of the polar distortion ξ over large (a) and small (b) ranges of ξ (note the different units on the energy axis). Here $\xi = 1$ corresponds to the ferroelectric bulk structure, the energy minimum in our calculations, with P$_\xi$=11 μC/cm^2 (details in the SM [29]). The energy zero is set at $\xi = 0$, which corresponds to the structure with the atoms at their centrosymmetric positions. The atomic positions are interpolated linearly between their values at $\xi = 0$ and $\xi = 1$ and extrapolated linearly to larger values of ξ, with all three lattice parameters fixed, for all values of ξ, to those of the fully relaxed ferroelectric unit cell [30]. As expected, our zero kelvin DFT calculations, which do not include the quantum mechanical zero-point energy, give a characteristic ferroelectric double-well potential with a very small energy barrier (below 0.2 meV) between the oppositely polarized states. Solution of the Schrödinger equation using this potential has its lowest energy eigenvalue above the height of the barrier [31]. The DFT description, while of course not capturing explicitly the suppression of ferroelectricity by quantum fluctuations in the low-temperature state [32], is therefore consistent with quantum paraelectric behavior.

B. KTaO$_3$ thin films

Having established that our DFT setup provides a good description of bulk KTaO$_3$, we now turn to thin films. We construct a four-unit-cell-thick stoichiometric slab of cubic paraelectric KTaO$_3$ as described in the Methods section, placing the negatively charged KO layer on the top and the positively charged TaO$_2$ layer on the bottom as shown in Fig. 3(a). In the paraelectric structure, only the layer
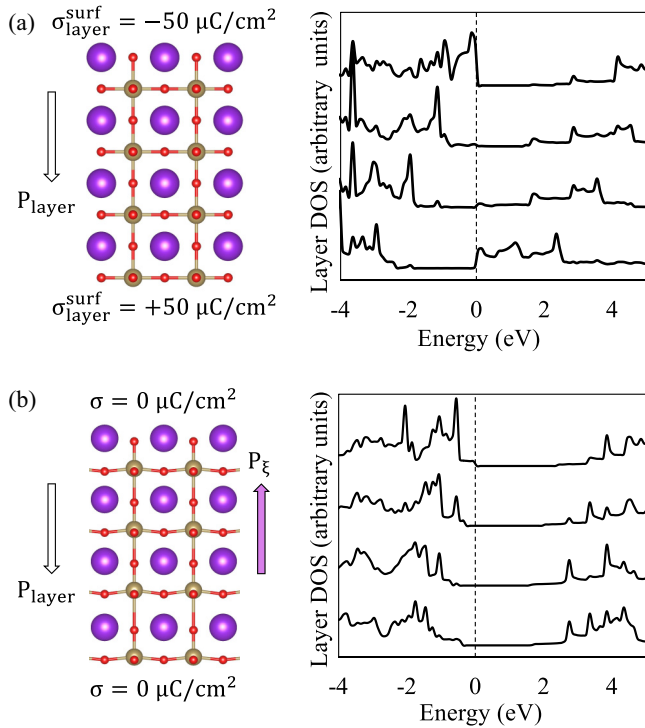
FIG. 3. Structure, left, and layer-by-layer DOS, right, for (a) cubic paraelectric and (b) fully relaxed four-unit-cell (001) KTaO$_3$ slab. The orientation of the layer polarization P_{layer} producing the layer surface charges $\sigma_{\text{layer}} = \pm 50 \mu C/cm^2$ is indicated with white arrows. In (a) the band bending in the layer-by-layer DOS in the right panel is due to the generation of electron-hole pairs across the band gap. In (b) the surface charge is compensated by the ferroelectriclike polarization P_{ξ} (purple arrows), which can be seen in the relative displacements of the ions.

polarization contributes to the surface charge, which, as shown in Fig. 1, has a value of $-0.5e$ per unit cell area on the KO surface and $+0.5e$ per unit cell area on the TaO$_2$ surface. This converts to $\pm 50 \mu C/cm^2$ at our calculated bulk lattice constant of 4.026Å. An additional polarization from a ferroelectriclike polar lattice distortion along the [001] direction $P_{\xi}^{[001]}$ of $\pm 50 \mu C/cm^2$ would therefore fully compensate the surface charge from the layer polarization.

Indeed, when we fully relax the atomic positions in the slab, with the in-plane lattice constant fixed to our calculated bulk value (4.026 Å), we find that the lowest energy structure, shown in Fig. 3(b), develops a large ferroelectriclike polarization, with an average dipole moment per unit volume P_{ξ} close in value to the layer polarization of $50 \mu C/cm^2$. P_{ξ} points in the opposite direction of P_{layer}, so that its associated bound surface charges compensate those from the layer polarization. We note that while part of P_{ξ} originates from the 11 $\mu C/cm^2$ spontaneous polarization seen in our potential energy calculation of Fig. 2, the majority is induced by the polarizing field caused by the uncompensated surface charges associated with the large layer polarization.

The electrostatic force driving the development of the ferroelectriclike induced polarization can be seen in the calculated layer-by-layer densities of states (DOS) in the right panels of Fig. 3. Figure 3(a) shows the layer-by-layer DOS
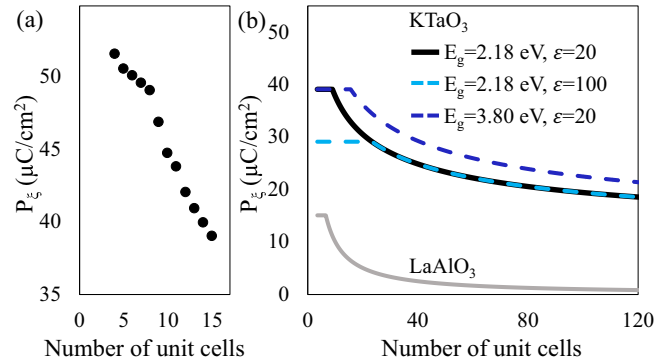

FIG. 4. Ferroelectriclike polarization P_{ξ} for KTaO$_3$ slabs as a function of slab thickness, calculated (a) with DFT and (b) using the electrostatic model of Eq. (6). The band gap (E_g) and dielectric constant ϵ used in the model are shown in the figure. The polarization for LaAlO$_3$, with the DFT-computed band gap $E_g = 4.10$ eV, and $\epsilon = 25$ is also shown (gray line).

across the slab in the paraelectric case. The uncompensated layer surface charges result in a large internal electric field, which can be seen in the bending of the energy bands across the slab. The Fermi energy (at 0 eV) lies in the conduction band at the lower (positively charged) surface layer, and in the valence band at the upper (negatively charged) surface layer, providing electrons in the conduction band of the bottom layer, which compensate the positive TaO$_2$ layer charge, and holes in the valence band of the top KO layer to compensate the negative surface layer charge. Figure 3(b) shows the analogous layer-by-layer DOS for the relaxed structure, in which P_{ξ} compensates the layer polarization. In striking contrast to the paraelectric slab, the internal electric field and corresponding band bending are minimal.

In Fig. 4(a) we show our DFT-calculated ferroelectriclike polarization P_{ξ} for slabs of increasing thickness. P_{ξ} remains approximately equal to $-P_{\text{layer}}$ until a thickness of eight unit cells, when it starts to decrease; the crossover corresponds to the thickness at which compensating surface charges are generated via electron-hole excitation across the band gap (see SM [29]). Even at the largest thickness that is practical in our calculations (15 unit cells), we find a drop of the P_{ξ} value of only $\sim 10 \mu C/cm^2$ from its maximum.

C. Electrostatic model

We now present a simple model to estimate the polarization induced by a polarizing field in slabs of arbitrary thickness, given a particular lattice polarization, energy versus polar distortion profile, and screening mechanism. The model contains the following contributions:

(a) Bulk polarization energy. We describe the internal energy per unit volume E_{int} as a function of the polarization arising from the ferroelectriclike distortion P_{ξ} in the usual Landau form:

$$E_{\text{int}} = aP_{\xi}^2 + bP_{\xi}^4 \quad . \tag{2}$$

The energy per unit surface area from this contribution is then $E_{\text{int}}d$, where d is the film thickness. Fitting to our calculated energy versus P_{ξ} profile over the range $-7 \leqslant \xi \leqslant 7$

gives $a = -2.816 \times 10^{-3}$ meV cm$^4\mu$C^{-2} and $b = 1.123 \times 10^{-5}$ meV cm$^8\mu$C^{-4}.

(b) Electrostatic energy from any unscreened polarization perpendicular to the slab surface. The net polarization contributing to the electrostatic energy is the layer polarization P_{layer} minus any ferroelectriclike polarization P_{ξ} that opposes it, further reduced by any charge accumulation on the surface from additional screening mechanisms. The net polarization causes a polarizing field,

$$\mathcal{E}_{\text{pol}} = \frac{1}{\epsilon_0 \epsilon_r}(P_{\text{layer}} - P_{\xi} - \sigma_{\text{scr}}), \tag{3}$$

which results in an electrostatic energy per unit area E_{es} of

$$E_{\text{es}} = \frac{1}{2\epsilon_0 \epsilon_r}(P_{\text{layer}} - P_{\xi} - \sigma_{\text{scr}})^2 d \quad , \tag{4}$$

where σ_{scr} is the magnitude of the screening charge per unit area on each surface.

(c) Screening energy. Following Ref. [5], we assume generation of electron-hole pairs across the gap as the screening mechanism. Thus, the screening energy per unit area E_{scr} is given by

$$E_{\text{scr}} = \frac{\sigma_{\text{scr}}}{e}E_g \quad . \tag{5}$$

Here e is the size of the electronic charge and E_g is the band gap (in electron volts). This screening mechanism is the only one available to a pristine system in vacuum and provides an upper bound to the screening energy for a real system, in which lower energy screening processes associated with point defects or adsorbates [10] are likely available.

The total energy per unit area of the slab is the sum of these three contributions:

$$\begin{aligned}E_{\text{tot}} &= E_{\text{int}}d + E_{\text{es}} + E_{\text{scr}} \\ &= \left(aP_{\xi}^2 + bP_{\xi}^4\right)d + \frac{(P_{\text{layer}} - P_{\xi} - \sigma_{\text{scr}})^2}{2\epsilon_0 \epsilon_r}d + \frac{\sigma_{\text{scr}}}{e}E_g.\end{aligned} \tag{6}$$

Note that the internal and electrostatic energies have the same dependence on slab thickness d, and so in the absence of electron-hole excitations across the gap, P_{ξ} is not thickness-dependent.

We then calculate the values of P_{ξ} and σ_{scr} that minimize this total energy for each value of d, noting that there is a critical thickness for the formation of screening electron-hole pairs because of the finite size of the band gap. The detailed derivation and the MATLAB code are provided in the SM [29]. Our calculated P_{ξ} as a function of slab thickness for our calculated band gap $E_g = 2.18$ eV and a representative value of the relative permittivity $\epsilon_r = 20$ is shown in Fig. 4(b) (black solid line) for the formal charge value of $P_{\text{layer}} = 50$ μC/cm^2. We find good agreement between the model and DFT behaviors, with P_{ξ} constant at a value close to the layer polarization for small slab thicknesses at which screening charges are not generated, and decreasing above a critical thickness of eight unit cells when it becomes energetically favorable to excite screening charges across the band gap. For comparison we also show the model calculation using the experimental band gap of $E_g = 3.8$ eV (blue dashed line) and with the calculated

band gap but with $\epsilon_r = 100$ (cyan dashed line). As expected, the larger experimental band gap increases the energy cost of screening through electron-hole excitation across the gap, so the saturation polarization persists to larger thickness, whereas the larger dielectric constant reduces the size of the polarizing field and hence lowers the saturation polarization. In all cases P_{ξ} reaches its lower limit (the spontaneous polarization at the energy minima of Fig. 2) only at thicknesses of several microns, indicating that the physics described here is valid for films far beyond the ultrathin limit.

Finally, we compare the behavior of KTaO$_3$ with that of LaAlO$_3$ [gray solid line in Fig. 4(b)], which also contains layer charges and which has been discussed extensively in the literature in the context of its conducting interface with SrTiO$_3$ [9]. LaAlO$_3$ is a robust paraelectric; its energy landscape has a minimum for the centrosymmetric phase and increases rapidly with increasing polarization (see SM [29]). As a result, the first term in Eq. (6) is large, and LaAlO$_3$ maintains a polarization only for ultrathin films. The blue line in Fig. 4(b) shows the model behavior using our calculated values of a, b and band gap (see SM [29] for details), and the experimental dielectric permittivity $\epsilon_r = 25$. This hardness of the polar mode [33] is of course favorable for the production of the interfacial two-dimensional electron gas, the formation of which is a lower energy process than the polarization of LaAlO$_3$[30]. Conversely, we anticipate that the formation of a conducting two-dimensional electron gas at a KTaO$_3$-SrTiO$_3$ interface will be less favorable [34].

IV. DISCUSSION

In summary, we have shown that thin films of insulating materials with charged ionic layers have an intrinsic *polarizing field* that can drive the formation of a ferroelectriclike induced polarization in otherwise paraelectric materials. This polarizing field derives from the same physics—the drive to compensate bound surface charges—as the *depolarizing* field of ferroelectric materials, but manifests in the opposite way, by inducing polarization in the paraelectric phase rather than suppressing the polarization of a ferroelectric. The effect manifests when the paraelectric state has a surface charge associated with a component of the bulk layer polarization lattice [6] perpendicular to the surface normal, and when the internal energy cost to deform the ground-state paraelectric structure into a polar state is not large. We illustrated the behavior using [001]-oriented films of stoichiometric KTaO$_3$ with flat (001) surfaces, for which our DFT calculations yield a polar ground state up to the thickness limit (15 unit cells) accessible in our computations. The induced polarization points away from the TaO$_2^+$ and toward the KO$^-$ surface so that its associated surface charge partially compensates that from the charged ionic layers. Finally, we introduced an electrostatic model that indicates that the ferroelectriclike polarization persists in KTaO$_3$ up to thicknesses of several microns and that is easily generalizable to other materials and to other compensation mechanisms [1–5,7].

The case of KTaO$_3$ is particularly relevant in light of recent experiments suggesting an influence of the surface orientation

on superconductivity. Using the method presented above to calculate the layer polarization and the corresponding surface charge, we see that for the low-Miller-index planes, the surface charges associated with the bulk layer polarization for *flat* surfaces or interfaces follow the trend $\sigma_{\text{surf}}^{(111)} > \sigma_{\text{surf}}^{(110)} > \sigma_{\text{surf}}^{(001)}$. Consistent with the need to screen the associated polar discontinuities, the surfaces readily form two-dimensional electron gases that have been well characterized using angle-resolved photoemission [17,35,36]. (Note that an interface of $KTaO_3$ is electrostatically similar to a surface, provided that its neighbor is not a coherent I-V perovskite oxide, and so we use the term surface also for interfaces with systems that are not the vacuum.) These surface two-dimensional electron gases become superconducting at low temperature, with different reported superconducting critical temperatures T_c for each of the three orientations. Intriguingly, the (111) surfaces have the highest reported T_c (2.2 K) [21], followed by 0.9 K for (110) [20] and 50 mK for (001) [19] surfaces, following the same trend as the surface charges associated with the bulk layer polarization. Detailed investigation of the structure of the surfaces of superconducting $KTaO_3$ samples in the three orientations is therefore of utmost interest. We note in particular that both the (110) and (111) surfaces are able to lower their surface charges by forming steps [in the (110) case an uncharged surface is even possible from such rearrangements], and that such behavior is likely.

While $KTaO_3$ is particularly suitable for illustrating the consequences of the polarizing field for the reasons discussed above, some degree of induced polarization is likely in thin enough films of all materials that have a surface charge associated with a layer polarization, with the thickness for which

an induced polarization is maintained determined by the balance of contributions to the total energy given in Eq. (6). Among perovskite-structure oxides, the flat (001) and (111) surfaces of III-III and I-V structures are all candidates. As mentioned above, induced polarization plays a small role in compensating the polar discontinuity at the $LaAlO_3$-$SrTiO_3$ interface [37], although the formation of the 2DEG dominates the physics.

Finally, we note that the behavior we describe is robust to, and can even be slightly favored by, biaxial strain introduced through coherent heteroepitaxy, which modifies the balance of the contributions to the total energy by changing the unit-cell surface area and tuning the a and b parameters in E_{int}. In this context, the concepts discussed here could be particularly relevant for thin-film growth processes, with the fabrication of ultrathin films in orientations corresponding to charged surfaces likely less prohibitive than previously expected. We hope that our work inspires experimental efforts to demonstrate, characterize, and exploit the polarizing field in thin-film $KTaO_3$ and related materials.

[1] P. Wurfel and I. P. Batra, Depolarization-field-induced instability in thin ferroelectric films—Experiment and theory, Phys. Rev. B **8**, 5126 (1973).

[2] M. Dawber, K. M. Rabe, and J. F. Scott, Physics of thin-film ferroelectric oxides, Rev. Mod. Phys. **77**, 1083 (2005).

[3] C. Lichtensteiger, M. Dawber, N. Stucki, J.-M. Triscone, J. Hoffman, J.-B. Yau, C. H. Ahn, L. Despont, and P. Aebi, Monodomain to polydomain transition in ferroelectric $PbTiO_3$ thin films with $La_{0.67}Sr_{0.3}MnO_3$ electrodes, Appl. Phys. Lett. **90**, 052907 (2007).

[4] J. Junquera and P. Ghosez, Critical thickness for ferroelectricity in perovskite ultrathin films, Nature (London) **422**, 506 (2003).

[5] J. A. Mundy, B. F. Grosso, C. A. Heikes, D. F. Segedin, Z. Wang, Y.-T. Shao, C. Dai, B. H. Goodge, Q. N. Meier, C. T. Nelson, B. Prasad, F. Xue, S. Ganschow, D. A. Muller, L. F. Kourkoutis, L.-Q. Chen, W. D. Ratcliff, N. A. Spaldin, R. Ramesh, and D. G. Schlom, Liberating a hidden antiferroelectric phase with interfacial electrostatic engineering, Sci. Adv. **8**, eabg5860 (2022).

[6] M. Stengel, Electrostatic stability of insulating surfaces: Theory and applications, Phys. Rev. B **84**, 205432 (2011).

[7] A. Ohtomo and H. Y. Hwang, A high-mobility electron gas at the $LaAlO_3$/$SrTiO_3$ heterointerface, Nature (London) **427**, 423 (2004).

[8] H. Y. Hwang, Tuning interface states, Science **313**, 1895 (2006).

[9] N. Nakagawa, H. Y. Hwang, and D. A. Muller, Why some interfaces cannot be sharp, Nat. Mater. **5**, 204 (2006).

[10] S. M. Yang, A. N. Morozovska, R. Kumar, E. A. Eliseev, Y. Cao, L. Mazet, N. Balke, S. Jesse, R. K. Vasudevan, C. Dubourdieu, and S. V. Kalinin, Mixed electrochemical-ferroelectric states in nanoscale ferroelectrics, Nat. Phys. **13**, 812 (2017).

[11] I. Efe, N. A. Spaldin, and C. Gattinoni, On the happiness of ferroelectric surfaces and its role in water dissociation: The example of bismuth ferrite, J. Chem. Phys. **154**, 024702 (2021).

[12] N. A. Spaldin, I. Efe, M. Rossell, and C. Gattinoni, Layer and spontaneous polarizations in perovskite oxides and their interplay in multiferroic bismuth ferrite, J. Chem. Phys. **154**, 154702 (2021).

[13] D. E. E. Deacon-Smith, D. O. Scanlon, C. R. A. Catlow, A. A. Sokol, and S. M. Woodley, Interlayer cation exchange stabilizes polar perovskite surfaces, Adv. Mater. **26**, 7252 (2014).

[14] M. Setvin, M. Reticcioli, F. Poelzleitner, J. Hulva, M. Schmid, L. A. Boatner, C. Franchini, and U. Diebold, Polarity compensation mechanisms on the perovskite surface $KTaO_3$(001), Science **359**, 572 (2018).

[15] Y. Wang, J. Cheng, M. Behtash, W. Tang, J. Luo, and K. Yang, First-principles studies of polar perovskite $KTaO_3$ surfaces: Structural reconstruction, charge compensation, and stability diagram, Phys. Chem. Chem. Phys. **20**, 18515 (2018).

[16] X. Zhao and A. Selloni, Structure and stability of NaTaO₃(001) and KTaO₃(001) surfaces, Phys. Rev. Mater. **3**, 015801 (2019).

[17] P. D. C. King, R. H. He, T. Eknapakul, P. Buaphet, S.-K. Mo, Y. Kaneko, S. Harashima, Y. Hikita, M. S. Bahramy, C. Bell, Z. Hussain, Y. Tokura, Z.-X. Shen, H. Y. Hwang, F. Baumberger, and W. Meevasana, Subband Structure of a Two-Dimensional Electron Gas Formed at the Polar Surface of the Strong Spin-Orbit Perovskite KTaO₃, Phys. Rev. Lett. **108**, 117602 (2012).

[18] A. F. Santander-Syro, C. Bareille, F. Fortuna, O. Copie, M. Gabay, F. Bertran, A. Taleb-Ibrahimi, P. Le Fèvre, G. Herranz, N. Reyren, M. Bibes, A. Barthélémy, P. Lecoeur, J. Guevara, and M. J. Rozenberg, Orbital symmetry reconstruction and strong mass renormalization in the two-dimensional electron gas at the surface of KTaO₃, Phys. Rev. B **86**, 121107(R) (2012).

[19] K. Ueno, S. Nakamura, H. Shimotani, H. T. Yuan, N. Kimura, T. Nojima, H. Aoki, Y. Iwasa, and M. Kawasaki, Two-dimensional superconductivity and anisotropic transport at KTaO₃(111) interfaces, Nat. Nanotechnol. **6**, 408 (2011).

[20] Z. Chen, Z. Liu, Y. Sun, X. Chen, Y. Liu, H. Zhang, H. Li, M. Zhang, S. Hong, T. Ren, C. Zhang, H. Tian, Y. Zhou, J. Sun, and Y. Xie, Two-Dimensional Superconductivity at the LaAlO₃/ KTaO₃(110) Heterointerface, Phys. Rev. Lett. **126**, 026802 (2021).

[21] C. Liu, X. Yan, D. Jin, Y. Ma, H.-W. Hsiao, Y. Lin, T. M. Bretz-Sullivan, X. Zhou, J. Pearson, B. Fisher, J. S. Jiang, W. Han, J.-M. Zuo, J. Wen, D. D. Fong, J. Sun, H. Zhou, and A. Bhattacharya, Two-dimensional superconductivity and anisotropic transport at KTaO₃(111) interfaces, Science **371**, 716 (2021).

[22] J. H. Barrett, Dielectric constant in perovskite type crystals, Phys. Rev. **86**, 118 (1952).

[23] S. H. Wemple, Some transport properties of oxygen-deficient single-crystal potassium tantalate (KTaO₃), Phys. Rev. **137**, A1575 (1965).

[24] S. E. Rowley, L. J. Spalek, R. P. Smith, M. P. M. Dean, M. Itoh, J. F. Scott, G. G. Lonzarich, and S. S. Saxena, Ferroelectric quantum criticality, Nat. Phys. **10**, 367 (2014).

[25] P. Giannozzi, S. Baroni, N. Bonini, M. Calandra, R. Car, C. Cavazzoni, D. Ceresoli, G. L. Chiarotti, M. Cococcioni, I. Dabo, A. D. Corso, S. de Gironcoli, S. Fabris, G. Fratesi, R. Gebauer, U. Gerstmann, C. Gougoussis, A. Kokalj, M. Lazzeri, L. Martin-Samos *et al.*, QUANTUM ESPRESSO: A modular and open-source software project for quantum simulations of materials, J. Phys.: Condens. Matter **21**, 395502 (2009).

[26] J. P. Perdew, K. Burke, and M. Ernzerhof, Generalized Gradient Approximation Made Simple, Phys. Rev. Lett. **77**, 3865 (1996).

[27] K. F. Garrity, J. W. Bennett, K. M. Rabe, and D. Vanderbilt, Pseudopotentials for high-throughput DFT calculations, Comput. Mater. Sci. **81**, 446 (2014).

[28] S. Cabuk, Ab initio volume-dependent elastic and lattice dynamics properties of KTaO₃, Phys. Status Solidi B **247**, 93 (2010).

[29] See Supplemental Material at http://link.aps.org/supplemental/10.1103/PhysRevResearch.4.L032020 for detailed calculations of bulk and slab KTaO₃, the polarization-energy profile of LaAlO₃, and the detailed solution and code for Eq. (6)

[30] Note that changes in the details of the calculation, such as using the lattice parameter of the paraelectric unit cell, or relaxing the lattice axis in the direction of the polar distortion lead to small changes in the shape of the double well. The exact procedure does not, however, affect our findings.

[31] T. Esswein and N. A. Spaldin, Ferroelectric, quantum paraelectric or paraelectric? Calculating the evolution from BaTiO₃ to SrTiO₃ to KTaO₃ using a single-particle quantum-mechanical description of the ions, Phys. Rev. Research, **4**, 033020 (2022).

[32] A. R. Akbarzadeh, L. Bellaiche, K. Leung, J. Íñiguez, and D. Vanderbilt, Atomistic simulations of the incipient ferroelectric KTaO₃, Phys. Rev. B **70**, 054103 (2004).

[33] M. V. Abrashev, A. P. Litvinchuk, M. N. Iliev, R. L. Meng, V. N. Popov, V. G. Ivanov, R. A. Chakalov, and C. Thomsen, Comparative study of optical phonons in the rhombohedrally distorted perovskites LaAlO₃ and LaMnO₃, Phys. Rev. B **59**, 4146 (1999).

[34] We note that previous DFT calculations of SrTiO₃-LaAlO₃ heterostructures overestimated the polarizability of the LaAlO₃ as a result of disabling its large octahedral rotations [37]; this considerably softens the polar mode leading to an underestimation of the energy cost to polarize (see SM [29]). In spite of this, the LaAlO₃ still showed considerable band bending, and charge transfer across the gap, even in the ultra-thin limit.

[35] F. Y. Bruno, S. McKeown Walker, S. Ricco, A. de la Torre, Z. Wang, A. Tamai, T. K. Kim, M. Hoesch, M. S. Bahramy, and F. Baumberger, Band structure and spinorbital texture of the (111)-KTaO₃ 2D electron gas, Adv. Electron. Mater. **5**, 1800860 (2019).

[36] C. Bareille, F. Fortuna, T. C. Rödel, F. Bertran, M. Gabay, O. H. Cubelos, A. Taleb-Ibrahimi, P. L. Fèvre, M. Bibes, A. Barthélémy, T. Maroutian, P. Lecoeur, M. J. Rozenberg, and A. F. Santander-Syro, Two-dimensional electron gas with sixfold symmetry at the (111) surface of KTaO₃, Sci. Rep. **4**, 3586 (2015).

[37] R. Pentcheva and W. E. Pickett, Avoiding the Polarization Catastrophe in LaAlO₃ Overlayers on SrTiO₃(001) through Polar Distortion, Phys. Rev. Lett. **102**, 107602 (2009).